

# PHOTOCATALYTIC DISCOLORATION OF REACTIVE BLUE 5G DYE IN THE PRESENCE OF MIXED OXIDES AND WITH THE ADDITION OF IRON AND SILVER

M. C. P. Souza<sup>1</sup>, G. G Lenzi<sup>1\*</sup>, L. M. S. Colpini<sup>2</sup>, L. M. M. Jorge<sup>1</sup> and O. A. A. Santos<sup>1</sup>

<sup>1</sup>Universidade Estadual de Maringá, Departamento de Engenharia Química,  
Phone: + (55) (44) 3011-4770, Fax: + (55) (44) 3011-4792,  
Av. Colombo 5790, CEP: 87020-900, Maringá - PR, Brazil.  
E-mail: gianegoncalves@hotmail.com

<sup>2</sup>Universidade Federal do Paraná, Campus Palotina,  
Curso Superior de Tecnologia em Biocombustíveis, Rua Pioneiro 2153,  
Jardim Dallas, CEP: 85950-000, Palotina - PR, Brazil.

(Submitted: December 12, 2010 ; Revised: May 18, 2011 ; Accepted: May 18, 2011)

**Abstract** - This work reports the use of cerium-titania-alumina-based systems modified with Ag and Fe by the wetness impregnation method for the discoloration of blue 5G dye. The techniques employed to characterize the photocatalysts were: temperature-programmed reduction (TPR), X-ray diffraction (XRD), specific surface area, average pore volume, and average pore diameter. The characterization results indicated that the photocatalysts had different crystalline structures and textural properties. Discoloration with the mixed oxide photocatalyst CeO<sub>2</sub>-TiO<sub>2</sub>-Al<sub>2</sub>O<sub>3</sub> gave a result similar to that of TiO<sub>2</sub>. On the other hand, the addition of Ag and Fe to the mixed oxide increased the discoloration and reaction rates of reactive blue 5G dyes.

**Keywords:** CeO<sub>2</sub>-TiO<sub>2</sub>-Al<sub>2</sub>O<sub>3</sub> mixed oxides; Discoloration; Fe-CeO<sub>2</sub>-TiO<sub>2</sub>-Al<sub>2</sub>O<sub>3</sub>; Ag-CeO<sub>2</sub>-TiO<sub>2</sub>-Al<sub>2</sub>O<sub>3</sub>; Reactive blue 5G dye; Characterization.

## INTRODUCTION

Textile dyes and other industrial dyes are crucial organic compounds that cause an increase in environmental damage. From about 1% to 20% of the world's dye production is wasted during the dyeing processes and released in textile effluents (Konstantinou and Albanis, 2004; Zollinger, 1991; Weber and Stickney, 1993; Ràfols and Barceló, 1997; Houas *et al.*, 2001). Dyes make up an abundant class of organic compounds characterized by the presence of unsaturated groups (chromophores), such as -C=C-, -N=N- and -C≡N-, which are responsible for the dye colors, and functional groups responsible for their fixation to fibers, as for example

-NH<sub>2</sub>, -OH, -COOH and -SO<sub>3</sub>H (Molinari *et al.*, 2004). Due to the environmental impact of dye-containing effluents, new technologies have been researched for their degradation, such as heterogeneous photocatalysis, which belongs to the category of advanced oxidation processes (AOP) (Özkan *et al.*, 2004; Colpini *et al.*, 2008; Pelegrini *et al.*, 1999; Peralta-Zamora *et al.*, 2003). Titania is a material with attractive applications in photocatalysis. However, TiO<sub>2</sub> has band gaps of approximately 3.0-3.2 eV. The photocatalytic process must be induced by UV light irradiation. The extremely low surface coverage of organic pollutants on the catalyst TiO<sub>2</sub> is the key factor in its low photocatalytic efficiency (Chen and Ray, 1999).

---

\*To whom correspondence should be addressed

Thus, recent studies have focused on the modification of TiO<sub>2</sub> (Yan *et al.*, 2006). In order to investigate this further, mixed oxide (CeO<sub>2</sub>-TiO<sub>2</sub>- $\gamma$ -Al<sub>2</sub>O<sub>3</sub>) modified with Ag and Fe was prepared and characterized for the discoloration of blue 5G dye (Figure 1).

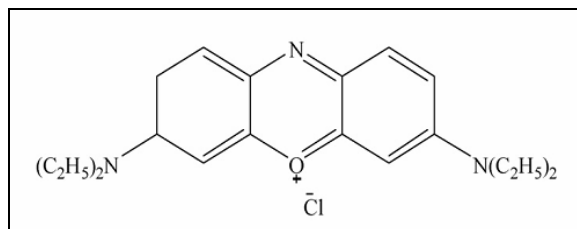


**Figure 1:** Structure of Maxilon Blue 5G.

## EXPERIMENTAL

### Chemicals

The following chemicals were used as received for the catalyst preparation: i) aluminum oxide Al<sub>2</sub>O<sub>3</sub> (supplied by Aldrich Sigma with over 99.9% purity); ii) titanium dioxide TiO<sub>2</sub> (supplied by Aldrich with over 99.9% purity) used as a catalyst precursor; iii) cerium CeO<sub>2</sub> IV (supplied by Acros Organics with over 99.9%); iv) iron(II) sulfate heptahydrate FeSO<sub>4</sub>.7H<sub>2</sub>O (supplied by Synth with over 99.9% purity); v) silver nitrate AgNO<sub>3</sub> (supplied by Synth with over 99.9% purity).

### Catalyst Preparation

To prepare the catalysts 8.8% Ag/CeO<sub>2</sub>-TiO<sub>2</sub>-Al<sub>2</sub>O<sub>3</sub> and 8.6% Fe/CeO<sub>2</sub>-TiO<sub>2</sub>-Al<sub>2</sub>O<sub>3</sub> by successive impregnation, the following methodology was used:

After calcining 5x10<sup>-3</sup> kg of  $\gamma$ -alumina at 473.15 K for 7200s under a static air atmosphere, it was wetted with distilled water (5x10<sup>-6</sup> m<sup>3</sup>) at room temperature and titanium dioxide (5x10<sup>-3</sup> kg) was added. The solution was stirred at room temperature for 43200 s for complete homogenization. It was then dried in an oven at 373.15 K for 43200 s and calcined at 473.15 K for 10800s under a static air atmosphere. The same procedure was used for cerium oxide (5x10<sup>-3</sup> kg). To the resulting sample, 7x10<sup>-6</sup> m<sup>3</sup> of distilled water and the metallic precursor were added (for the 8.8% Ag/CeO<sub>2</sub>-TiO<sub>2</sub>-Al<sub>2</sub>O<sub>3</sub> catalyst, 2.5x10<sup>-3</sup> kg AgNO<sub>3</sub> was added and for 8.6% Fe/CeO<sub>2</sub>-TiO<sub>2</sub>-Al<sub>2</sub>O<sub>3</sub> catalyst, 5x10<sup>-3</sup> kg FeSO<sub>4</sub>.7H<sub>2</sub>O was added) and then stirred at room temperature for 43200 s. Finally, the catalyst was dried in an oven at 373.15 K for 43200 s and calcined at 473.15 K and 623.15 K for 10800 s

under a static air atmosphere. For more details, see Souza (2009).

### Characterization

The characterization techniques used in this study were specific surface area, average pore diameter, pore volume, temperature programmed reduction, thermogravimetric analysis, and X-ray diffraction.

### Pore Properties (B.E.T. Method)

The pore properties, such as specific surface area, average pore diameter, and pore volume, were determined with a QUANTACHROME Analyzer – Model Nova-1200, using N<sub>2</sub> adsorption at 77 K. These analyses were carried out for calcined and non-calcined samples. Before analysis, the samples were submitted to thermal treatment at 573 K under vacuum for 7200 s to eliminate any water existing within the pores of the solids.

### Temperature Programmed Reduction (TPR)

The measurements were conducted in a home-built TPR apparatus using a quartz tube packed with the catalyst sample inside. The samples (65x10<sup>-6</sup> kg) were heated from room temperature to 1273.15 K at a heating rate of 4.72 K/s in a 1.75% H<sub>2</sub>/98.25% Ar gas flow at the rate of 5.0x10<sup>-7</sup> m<sup>3</sup>/s. The thermocouple was located in the central position of the bed and the results were obtained from the hydrogen consumption, which was recorded by a thermal conductivity detector.

### X-Ray Diffraction

The samples were measured in a Rigaku-Denki Diffractometer with Cu-K $\alpha$  radiation ( $\lambda$ = 1.5406 Å) at a voltage of 140 V and a current of 40 mA. The patterns obtained were then compared with the diffraction dataset cards from the Joint Committee of Powder Diffraction Standards (JCPDS, 1997).

### Photocatalytic Reaction

#### Photocatalysis

The reaction mixture was kept in a reactor consisting of a cylindrical Pyrex cell of 5.0x10<sup>-4</sup> m<sup>3</sup>. The tests were performed in 3600 s. The solution with 70 ppm of reactive blue 5G dye in the presence of 1 g of the photocatalyst (2 kg.m<sup>-3</sup>) was open to the air and an oxygen stream was bubbled into the

suspension at  $8.3 \times 10^{-9} \text{ m}^3 \cdot \text{s}^{-1}$ . A 125 W medium pressure mercury lamp, surrounded by a quartz thimble, was used for irradiation. In order to maintain room temperature, the vessel was surrounded by a jacket in which cold water flows. The reactor had a magnetic stirrer to ensure the homogeneity of the reaction mixture. At regular intervals, an aliquot of the suspension was withdrawn and filtered through a  $0.45 \text{ }\mu\text{m}$  Millipore filter. The discoloration of the solutions as a function of time was determined with a Shimadzu UV-1203 UV/Vis spectrophotometer. The color was the main parameter analyzed.

### Adsorption Behavior of Dyes and Photolysis

The adsorption tests were accomplished in the same system, but in the dark, according to Kansal *et al.* (2007). Experiments without a photocatalyst (i.e., photolysis only) were also carried out (Rezaee *et al.*, 2008).

## EXPERIMENTAL RESULTS

Table 1 shows the specific surface areas of  $\text{TiO}_2$ ,  $\text{CeO}_2$ ,  $\text{Al}_2\text{O}_3$  and  $\text{CeO}_2\text{-TiO}_2\text{-Al}_2\text{O}_3$ , as well as of the Ag- and Fe-doped catalysts before and after calcination (473.15 and 623.15 K), respectively. The results of specific volume and mean diameter of pores of  $\text{TiO}_2$ ,  $\text{CeO}_2$ ,  $\text{Al}_2\text{O}_3$ ,  $\text{CeO}_2\text{-TiO}_2\text{-Al}_2\text{O}_3$  and of the Ag- and Fe-doped catalysts before and after calcinations at 473.15 K and at 623.15 K (Table 2) are presented. Figures 2, 3 and 4 show the XRD profiles for  $\text{CeO}_2\text{-TiO}_2\text{-Al}_2\text{O}_3$ ,  $\text{Fe/CeO}_2\text{-TiO}_2\text{-Al}_2\text{O}_3$  and  $\text{Ag/CeO}_2\text{-TiO}_2\text{-Al}_2\text{O}_3$ , respectively. Figures 5 and 6 show the temperature-programmed reduction profiles for  $\text{CeO}_2$ ,  $\text{TiO}_2$ ,  $\text{Al}_2\text{O}_3$ ,  $\text{CeO}_2\text{-TiO}_2\text{-Al}_2\text{O}_3$ ,  $\text{Ag/CeO}_2\text{-TiO}_2\text{-Al}_2\text{O}_3$  and  $\text{Fe/CeO}_2\text{-TiO}_2\text{-Al}_2\text{O}_3$  calcined at 473.15 K and 623.15 K, respectively. Figures 7, 8 and 9 show the results for the adsorption of reactive blue 5G dye on the catalyst using  $\text{CeO}_2\text{-TiO}_2\text{-Al}_2\text{O}_3$ ,  $\text{Ag/CeO}_2\text{-TiO}_2\text{-Al}_2\text{O}_3$  and  $\text{Fe/CeO}_2\text{-TiO}_2\text{-Al}_2\text{O}_3$  photocatalysts, non-calcined and calcined at 473.15 K and 623.15 K, respectively. Figures 10, 11 and 12 show the discoloration of reactive blue 5G dyes with the photocatalyst, non-calcined and calcined at 473.15 K and at 623.15 K, respectively.

## DISCUSSION

The results (Table 1) indicate that the specific surface area of non-calcined materials follows the sequence  $\text{Al}_2\text{O}_3 > \text{CeO}_2 > \text{TiO}_2$ . When these three

oxides are combined, the specific surface area is  $8.0 \times 10^3 \text{ m}^2/\text{kg}$ , which is the same as that observed for  $\text{CeO}_2$ . With the addition of Ag, the surface area decreased, possibly due to pore blocking by the metal.

The surface area obtained for the catalyst containing Fe ( $4.7 \times 10^3 \text{ m}^2/\text{kg}$ ) is smaller than for Ag ( $5.3 \times 10^3 \text{ m}^2/\text{kg}$ ).

When the sample was calcined at 473.15 K,  $\text{TiO}_2$  presented an increase in specific surface area and external surface area, as compared with the non-calcined samples. For  $\text{Al}_2\text{O}_3$  and  $\text{Fe/CeO}_2\text{-TiO}_2\text{-Al}_2\text{O}_3$ , this difference is of the same order of magnitude as the experimental error. On the other hand, a decrease in the micropore surface area occurs. This is possibly due to the removal of volatile contaminants (Lenzi *et al.*, 2008), which favors an increase in the surface area, provoking sinterization of the catalyst particles and decreasing the micropore surface area.

For  $\text{CeO}_2$  and  $\text{Ag/CeO}_2\text{-TiO}_2\text{-Al}_2\text{O}_3$ , the specific surface area, external surface area and micropore area decreased, suggesting that some micropores form larger pores and contribute to the decrease in the specific surface area.

For the  $\text{CeO}_2\text{-TiO}_2\text{-Al}_2\text{O}_3$  catalyst, a decrease in the specific surface area and external surface area occurs. However, the micropore surface area increased due to the crystalline structure change produced by the thermal treatment. The results indicated a change in the specific surface after the thermal treatment (calcinations at 623.15 K). Compared with the non-calcined photocatalyst,  $\text{TiO}_2$  and  $\text{Al}_2\text{O}_3$  presented an increase in the specific surface area and specific external area. However, the specific micropore area decreased due to the removal of volatile contaminants. For the  $\text{Fe/CeO}_2\text{-TiO}_2\text{-Al}_2\text{O}_3$  photocatalyst, the specific surface area, external surface area, and micropore surface area were not significantly altered.

For  $\text{CeO}_2$ ,  $\text{CeO}_2\text{-TiO}_2\text{-Al}_2\text{O}_3$  and  $\text{Ag/CeO}_2\text{-TiO}_2\text{-Al}_2\text{O}_3$ , the specific surface area and specific external area decreased, and an increase in the micropore surface area occurred due to the crystalline structure change resulting from the thermal treatment.

$\text{TiO}_2$  shows high micropore volume (Table 2); however, the mesopore volume of the other oxides ( $\text{CeO}_2$ ,  $\text{Al}_2\text{O}_3$ ) and catalysts ( $\text{Ag/CeO}_2\text{-TiO}_2\text{-Al}_2\text{O}_3$ ,  $\text{Fe/CeO}_2\text{-TiO}_2\text{-Al}_2\text{O}_3$ ) was larger. The thermal treatment provoked changes in the pore volume and diameter. For  $\text{TiO}_2$  and  $\text{Al}_2\text{O}_3$ , an increase in the total pore volume and mesopore volume occurred, while the micropore volume decreased. The micropore volumes of  $\text{TiO}_2$  and  $\text{Al}_2\text{O}_3$  are practically the same and the difference is within the experimental error.

**Table 1: Specific surface area of TiO<sub>2</sub>, CeO<sub>2</sub>, Al<sub>2</sub>O<sub>3</sub>, CeO<sub>2</sub>-TiO<sub>2</sub>-Al<sub>2</sub>O<sub>3</sub>, Ag/CeO<sub>2</sub>-TiO<sub>2</sub>-Al<sub>2</sub>O<sub>3</sub> and Fe/CeO<sub>2</sub>-TiO<sub>2</sub>-Al<sub>2</sub>O<sub>3</sub>- non-calcined, calcined at 473.15 K, calcined at 623.15 K.**

Material	Total pore volume (m <sup>3</sup> /kg)			Micropore volume (m <sup>3</sup> /kg)			Micropore surface area (m <sup>2</sup> /kg) (10 <sup>3</sup> )		
	non-calcined	473.15 K	623.15 K	non-calcined	473.15 K	623.15 K	non-calcined	473.15 K	623.15 K
TiO <sub>2</sub>	5.4	10.5	12.0	0.5	7.5	8.0	4.9	3.0	4.0
CeO <sub>2</sub>	8.0	3.0	6.0	6.0	2.6	3.5	2.0	0.4	2.5
Al <sub>2</sub> O <sub>3</sub>	9.0	9.1	10.0	4.5	5.7	6.0	4.5	3.4	4.0
CeO <sub>2</sub> -TiO <sub>2</sub> -Al <sub>2</sub> O <sub>3</sub>	8.0	6.2	6.0	5.7	2.6	3.4	2.3	3.6	2.5
Ag/CeO <sub>2</sub> -TiO <sub>2</sub> -Al <sub>2</sub> O <sub>3</sub>	5.3	4.1	4.0	3.5	2.5	2.0	1.8	1.6	2.0
Fe/CeO <sub>2</sub> -TiO <sub>2</sub> -Al <sub>2</sub> O <sub>3</sub>	4.7	4.8	4.8	3.1	3.4	3.2	1.6	1.4	1.6

**Table 2: Specific volume and mean pore diameter of TiO<sub>2</sub>, CeO<sub>2</sub>, Al<sub>2</sub>O<sub>3</sub>, CeO<sub>2</sub>-TiO<sub>2</sub>-Al<sub>2</sub>O<sub>3</sub>, Ag/CeO<sub>2</sub>-TiO<sub>2</sub>-Al<sub>2</sub>O<sub>3</sub> and Fe/CeO<sub>2</sub>-TiO<sub>2</sub>-Al<sub>2</sub>O<sub>3</sub>- non-calcined, calcined at 473.15 K, calcined at 623.15 K.**

Material	Total pore volume (m <sup>3</sup> /kg)			Micropore volume (m <sup>3</sup> /kg)			Mesopore volume (m <sup>3</sup> /kg)			Mean pore diameter (Å)		
	non-calcined	473.15 K	623.15 K	non-calcined	473.15 K	623.15 K	non-calcined	473.15 K	623.15 K	non-calcined	473.15 K	623.15 K
TiO <sub>2</sub>	3.5	14.3	16.0	2.6	1.8	2.1	1.0	12.5	13.7	25	50	49
CeO <sub>2</sub>	11.0	5.8	7.4	1.0	1.0	1.3	10.0	4.8	6.0	23	53	25
Al <sub>2</sub> O <sub>3</sub>	10.5	11.5	12.8	2.5	1.8	2.3	8.0	9.7	10.5	42	45	48
CeO <sub>2</sub> -TiO <sub>2</sub> -Al <sub>2</sub> O <sub>3</sub>	10.2	7.0	7.3	1.2	2.0	1.3	10.0	5.0	6.0	51	37	50
Ag/CeO <sub>2</sub> -TiO <sub>2</sub> -Al <sub>2</sub> O <sub>3</sub>	7.0	5.5	4.6	1.0	0.9	1.1	6.0	4.5	3.5	47	48	44
Fe/CeO <sub>2</sub> -TiO <sub>2</sub> -Al <sub>2</sub> O <sub>3</sub>	6.7	6.7	6.6	0.7	0.7	0.7	6.0	6.0	5.9	49	51	51

The XRD patterns of the photocatalyst CeO<sub>2</sub>-TiO<sub>2</sub>-Al<sub>2</sub>O<sub>3</sub> (Fig. 2), non-calcined and calcined (473.15 and 623.15 K), indicated the formation of TiO<sub>2</sub> anatase, CeO<sub>2</sub> cerium oxide, and Al<sub>2</sub>O<sub>3</sub> corundum. The thermal treatment did not modify the structure of the mixed oxides. The addition of Fe did not alter the crystalline structure of the material (Fig. 3). However, when Ag was added, there appeared four small peaks (Fig. 4) which were attributed to AgNO<sub>3</sub>, which is possibly due to residual Ag precursor impregnated in the sample. The XRD results in general indicate essentially crystalline phases for the original Ce, Ti and Al oxides.

The temperature-programmed reduction (TPR) profile obtained for TiO<sub>2</sub> (Fig. 5b) and Al<sub>2</sub>O<sub>3</sub> (Fig. 5c) did not show hydrogen consumption or reduction in the peaks. For CeO<sub>2</sub> (Fig. 5a), one peak occurred

at around 973.15–1273.15 K, indicating the reduction of this material. For the mixed CeO<sub>2</sub>-TiO<sub>2</sub>-Al<sub>2</sub>O<sub>3</sub> oxides (Fig. 5d), the material presented one peak around 973.15 K, which had a lower intensity than in CeO<sub>2</sub>, perhaps due to the interaction with the other oxides (Al<sub>2</sub>O<sub>3</sub> and TiO<sub>2</sub>) and a possibly more difficult reduction. The Ag/CeO<sub>2</sub>-TiO<sub>2</sub>-Al<sub>2</sub>O<sub>3</sub> (Fig. 5e) photocatalyst presented two peaks at a low temperature, around 373.15–523.15 K and another at a high temperature of 523.15–773.15 K. These peaks indicate the reduction Ag<sup>2+</sup>→Ag<sup>+</sup>→Ag<sup>0</sup>. The Fe/CeO<sub>2</sub>-TiO<sub>2</sub>-Al<sub>2</sub>O<sub>3</sub> (Fig. 5f) material presented one high-intensity peak situated between 703.15 and 993.15 K, which was attributed to the reduction of Fe<sup>3+</sup> to Fe<sup>2+</sup>. The second broad small peak situated at 720–1273.15 K indicates the reduction Fe<sup>2+</sup>→Fe<sup>0</sup> and then cerium reduction.

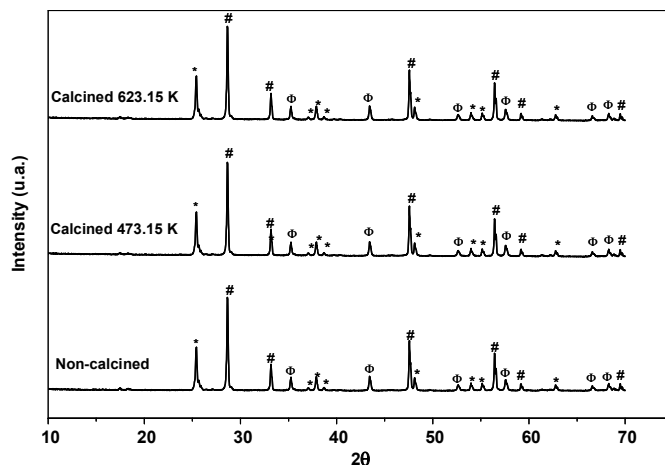


**Figure 2:** XRD pattern of the  $\text{CeO}_2\text{-TiO}_2\text{-Al}_2\text{O}_3$  samples, where: (\*)  $\text{TiO}_2$  anatase (JCPDS 21-1272), (#)  $\text{CeO}_2$  cerium oxide (JCPDS 78-0694) and ( $\Phi$ )  $\text{Al}_2\text{O}_3$  corundum (JCPDS 74-1081).

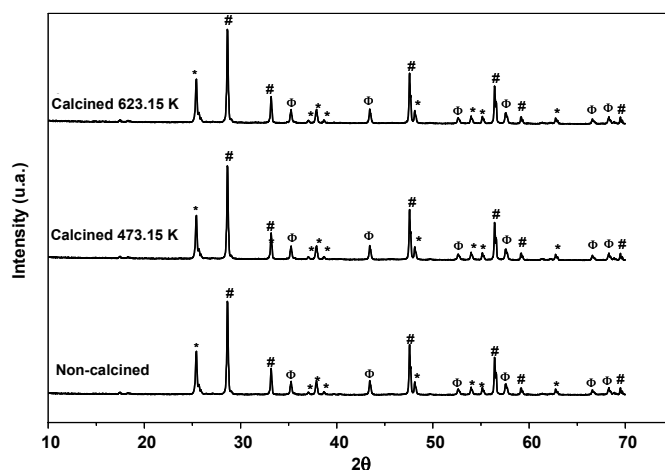


**Figure 3:** XRD pattern of the  $\text{Fe/CeO}_2\text{-TiO}_2\text{-Al}_2\text{O}_3$  samples, where: (\*)  $\text{TiO}_2$  anatase (JCPDS 21-1272), (#)  $\text{CeO}_2$  cerium oxide (JCPDS 78-0694) and ( $\Phi$ )  $\text{Al}_2\text{O}_3$  corundum (JCPDS 74-1081).

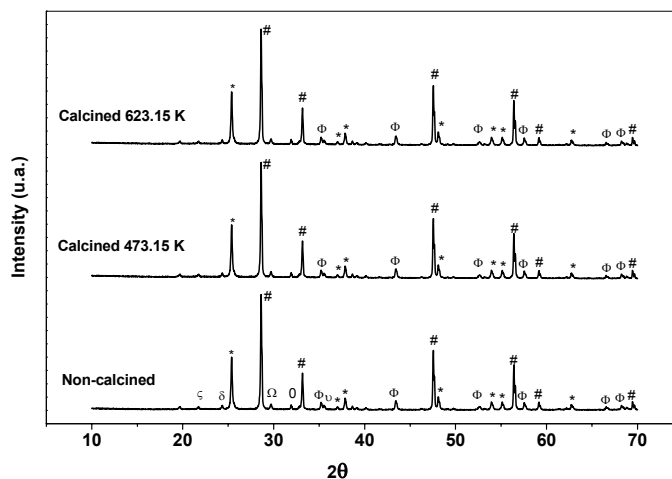


**Figure 4:** XRD pattern of the  $\text{Ag/CeO}_2\text{-TiO}_2\text{-Al}_2\text{O}_3$  samples, where: (\*)  $\text{TiO}_2$  anatase (JCPDS 21-1272), (#)  $\text{CeO}_2$  cerium oxide (JCPDS 78-0694), ( $\Phi$ )  $\text{Al}_2\text{O}_3$  corundum (JCPDS 74-1081) and ( $\delta$ )  $\text{AgNO}_3$  silver nitrate oxide (JCPDS 01-0856).

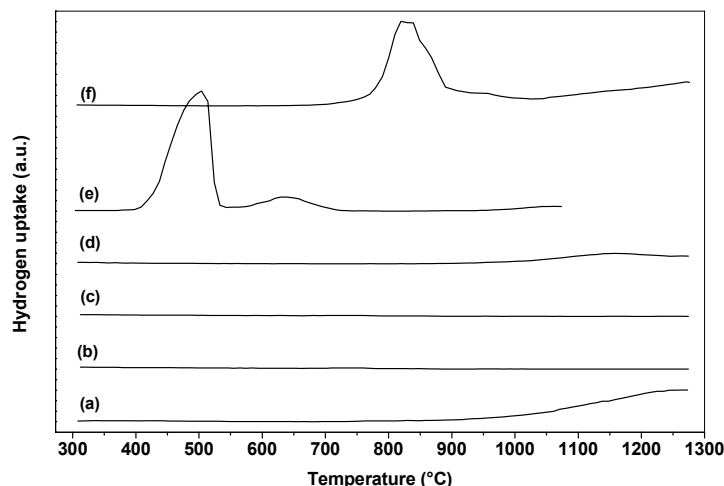


**Figure 5:** TPR for catalysts calcined at 473.15 K, where: (a) CeO<sub>2</sub>, (b) TiO<sub>2</sub>, (c) Al<sub>2</sub>O<sub>3</sub>, (d) CeO<sub>2</sub>-TiO<sub>2</sub>-Al<sub>2</sub>O<sub>3</sub>, (e) Ag/CeO<sub>2</sub>-TiO<sub>2</sub>-Al<sub>2</sub>O<sub>3</sub> and (f) Fe/CeO<sub>2</sub>-TiO<sub>2</sub>-Al<sub>2</sub>O<sub>3</sub>.

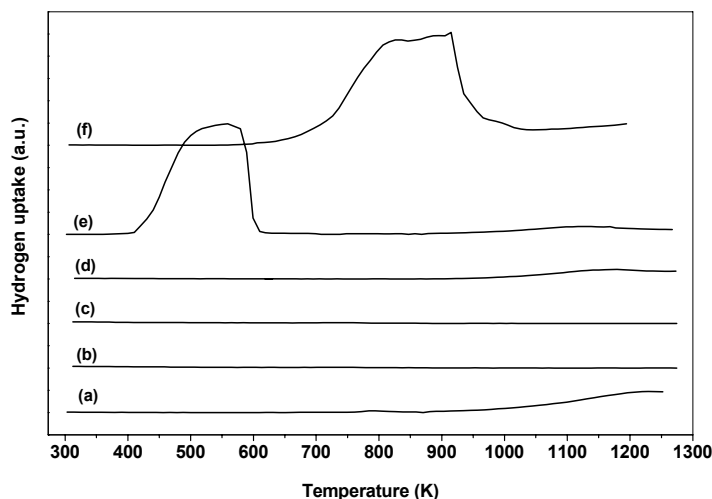


**Figure 6:** TPR for catalysts calcined at 623.15 K, where: (a) CeO<sub>2</sub>, (b) TiO<sub>2</sub>, (c) Al<sub>2</sub>O<sub>3</sub>, (d) CeO<sub>2</sub>-TiO<sub>2</sub>-Al<sub>2</sub>O<sub>3</sub>, (e) Ag/CeO<sub>2</sub>-TiO<sub>2</sub>-Al<sub>2</sub>O<sub>3</sub> and (f) Fe/CeO<sub>2</sub>-TiO<sub>2</sub>-Al<sub>2</sub>O<sub>3</sub>.

The TPR profiles of CeO<sub>2</sub>, TiO<sub>2</sub>, Al<sub>2</sub>O<sub>3</sub> and the CeO<sub>2</sub>-TiO<sub>2</sub>-Al<sub>2</sub>O<sub>3</sub> photocatalyst calcined at 623.15 K (Fig. 6) were similar to those of the materials calcined at 473.15 K. However, the profiles for Ag/CeO<sub>2</sub>-TiO<sub>2</sub>-Al<sub>2</sub>O<sub>3</sub> and Fe/CeO<sub>2</sub>-TiO<sub>2</sub>-Al<sub>2</sub>O<sub>3</sub> show broader peaks, indicating that this may be the result of a larger dispersion of these metals on the catalyst surface (Kansal *et al.*, 2007). For the photocatalyst Ag/CeO<sub>2</sub>-TiO<sub>2</sub>-Al<sub>2</sub>O<sub>3</sub>, the reduction Ag<sup>+</sup>→Ag<sup>0</sup> occurs.

The analysis of the adsorption tests (Fig. 7, 8 and 9) indicates that the presence of Fe favors greater discoloration and that its effect becomes more efficient as the calcination temperature increases,

with the largest adsorption being observed for the photocatalyst calcined at 623.15 K.

The CeO<sub>2</sub>-TiO<sub>2</sub>-Al<sub>2</sub>O<sub>3</sub> mixed-oxide photocatalysts calcined at 473.15 and 623.15 K had similar structures and surface areas. However, the photocatalyst calcined at 473.15 K presented a larger adsorption of reactive blue 5G dye due to its larger micropore surface area of 3.6×10<sup>3</sup> m<sup>2</sup>/kg as compared to 2.5×10<sup>3</sup> m<sup>2</sup>/kg when calcined at 623.15 K.

For TiO<sub>2</sub>, CeO<sub>2</sub>-TiO<sub>2</sub>-Al<sub>2</sub>O<sub>3</sub>, Ag/CeO<sub>2</sub>-TiO<sub>2</sub>-Al<sub>2</sub>O<sub>3</sub>, Al<sub>2</sub>O<sub>3</sub> and CeO<sub>2</sub>, the discoloration obtained by adsorption was approximately similar.

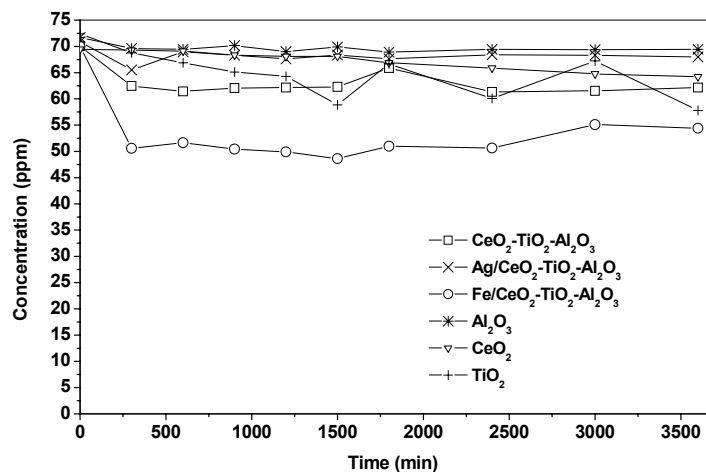


Figure 7: Adsorption of reactive blue 5G dye on non-calcined photocatalysts.

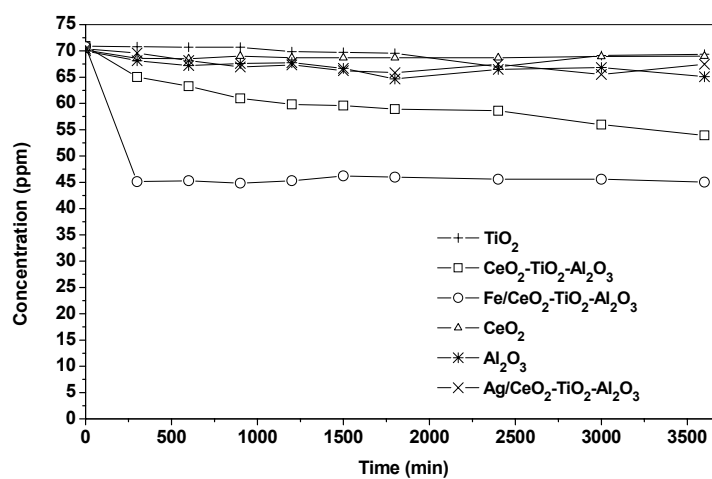


Figure 8: Adsorption of reactive blue 5G dye on photocatalyst calcined at 473.15 K.

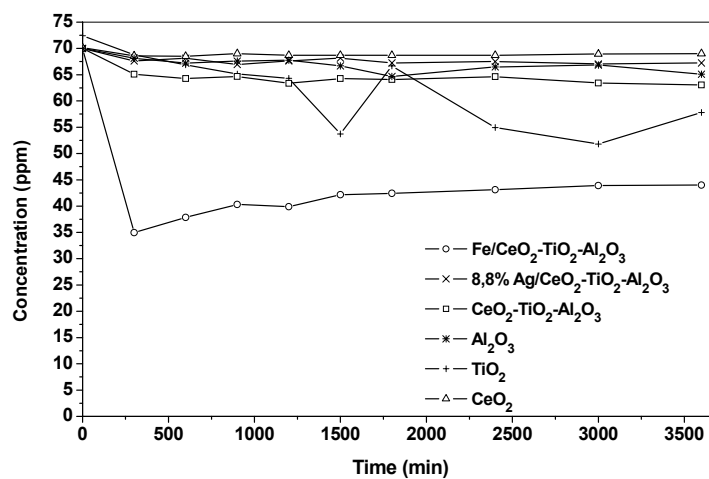


Figure 9: Adsorption of reactive blue 5G dye on photocatalyst calcined at 623.15 K.

The result for the photolysis test without a catalyst indicated a discoloration of the reactive blue 5G dye solution of around 8.57% in 3600 s.

The discoloration occurs quickly under these conditions for the photocatalyzed reactions, as observed in Figs. 10, 11 and 12, except for  $\text{Al}_2\text{O}_3$  and  $\text{CeO}_2$ . However, the discoloration times were different. This can be observed from the values inside the figures, which show the results of the kinetic study of the disappearance of the dyes for an initial concentration of  $70 \text{ kg/m}^3$ . The values show that the photocatalytic discoloration of dyes in an aqueous solution can be described by a first order kinetic model,  $\ln(C_0/C) = kt$ , where  $C_0$  is the initial concentration and  $C$  is the concentration at any  $t$  time.

The results for the non-calcined photocatalyst (Fig. 10) were better for  $\text{Fe/CeO}_2\text{-TiO}_2\text{-Al}_2\text{O}_3$  and  $\text{TiO}_2$ , which discolored 100% of the solution with 70 ppm of reactive blue 5G dye. The time for total discoloration (100%) was shorter for  $\text{Fe/CeO}_2\text{-TiO}_2\text{-Al}_2\text{O}_3$  (30 min).  $\text{CeO}_2$ ,  $\text{Al}_2\text{O}_3$ ,  $\text{CeO}_2\text{-TiO}_2\text{-Al}_2\text{O}_3$  and  $\text{Ag/CeO}_2\text{-TiO}_2\text{-Al}_2\text{O}_3$  produced 7.8%, 21.8%, 95.5% and 99.7% discoloration, respectively.

Figure 11 shows that the photocatalyst calcined at 473.15 K produced 100% discoloration of reactive blue 5G dye in this order:  $\text{Fe/CeO}_2\text{-TiO}_2\text{-Al}_2\text{O}_3 > \text{Ag/CeO}_2\text{-TiO}_2\text{-Al}_2\text{O}_3 > \text{TiO}_2$ . The reaction rate was different for each catalyst, and the shortest discoloration time was obtained for  $\text{Fe/CeO}_2\text{-TiO}_2\text{-Al}_2\text{O}_3$  with an apparent catalyst rate constant of  $3.5 \times 10^{-3} \text{ s}^{-1}$ . The  $\text{CeO}_2$ ,  $\text{Al}_2\text{O}_3$  and  $\text{CeO}_2\text{-TiO}_2\text{-Al}_2\text{O}_3$  oxides and mixed oxides produced 15.5, 14.3 and

96.3% discoloration, respectively.

Complete discoloration (100%) (Fig. 12) followed this order:  $\text{Fe/CeO}_2\text{-TiO}_2\text{-Al}_2\text{O}_3 > \text{Ag/CeO}_2\text{-TiO}_2\text{-Al}_2\text{O}_3 > \text{TiO}_2$  for the photocatalysts calcined at 623.15 K.  $\text{CeO}_2$ ,  $\text{Al}_2\text{O}_3$  and  $\text{CeO}_2\text{-TiO}_2\text{-Al}_2\text{O}_3$  showed discolorations of around 8.2, 21.6 and 96.4%, respectively.

It was observed that the time for discoloration was influenced by thermal treatment; when the calcinations temperature increased, the time of discoloration decreased. The modification of the specific surface area of the photocatalyst may have favored the photocatalytic discoloration under the conditions studied.

It can be observed in Figures 11 and 12 that the mixed oxides produced around 96% discoloration of reactive blue 5G dye in 3600 s of reaction time, while the oxide  $\text{TiO}_2$  produced 100%. However, with the addition of Fe, the discoloration time decreased to 15 min for  $\text{Fe/CeO}_2\text{-TiO}_2\text{-Al}_2\text{O}_3$  calcined at 473.15 K.

For the photocatalysts  $\text{TiO}_2$ ,  $\text{CeO}_2\text{-TiO}_2\text{-Al}_2\text{O}_3$ ,  $\text{CeO}_2$  and  $\text{Al}_2\text{O}_3$  calcined at different temperatures, no significant changes in discoloration time took place. Non-calcined  $\text{Ag/CeO}_2\text{-TiO}_2\text{-Al}_2\text{O}_3$  had similar characteristics (B.E.T. and XRD) after calcination, although the time of discoloration for the photocatalyst calcined at 623.15 K was shorter, possibly due to the larger elimination of contaminants from the surface of the photocatalyst, which may have favored the reaction.  $\text{Fe/CeO}_2\text{-TiO}_2\text{-Al}_2\text{O}_3$  catalysts calcined at 473.15 and 623.15 K had similar discoloration times.

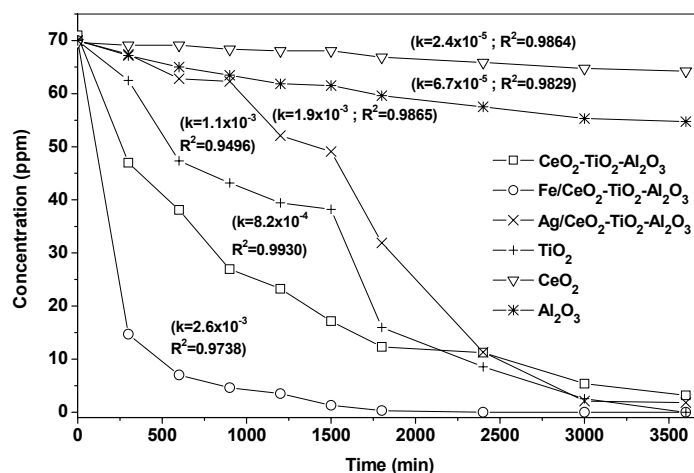


**Figure 10:** Photocatalytic discoloration of reactive blue 5G dye with  $\text{CeO}_2$ ,  $\text{TiO}_2$ ,  $\text{Al}_2\text{O}_3$  and  $\text{Fe/CeO}_2\text{-TiO}_2\text{-Al}_2\text{O}_3$  non-calcined photocatalysts.



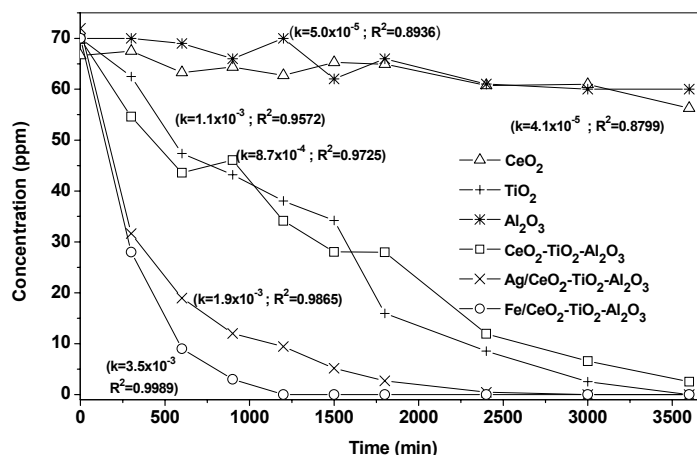


**Figure 11:** Photocatalytic discoloration of reactive blue 5G dye with CeO<sub>2</sub>, TiO<sub>2</sub>, Al<sub>2</sub>O<sub>3</sub>, CeO<sub>2</sub>-TiO<sub>2</sub>-Al<sub>2</sub>O<sub>3</sub>, Ag/CeO<sub>2</sub>-TiO<sub>2</sub>-Al<sub>2</sub>O<sub>3</sub> and Fe/CeO<sub>2</sub>-TiO<sub>2</sub>-Al<sub>2</sub>O<sub>3</sub> photocatalysts calcined at 473.15 K.

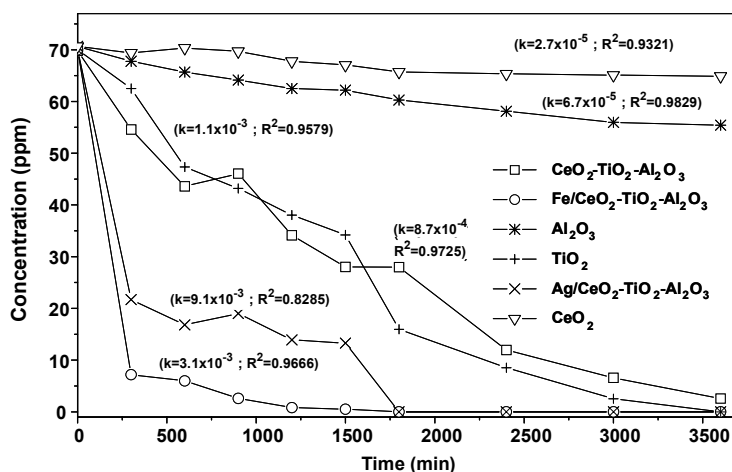


**Figure 12:** Photocatalytic discoloration of reactive blue 5G dye with CeO<sub>2</sub>, TiO<sub>2</sub>, Al<sub>2</sub>O<sub>3</sub>, CeO<sub>2</sub>-TiO<sub>2</sub>-Al<sub>2</sub>O<sub>3</sub>, Ag/CeO<sub>2</sub>-TiO<sub>2</sub>-Al<sub>2</sub>O<sub>3</sub> and Fe/CeO<sub>2</sub>-TiO<sub>2</sub>-Al<sub>2</sub>O<sub>3</sub> photocatalysts calcined at 623.15 K.

## CONCLUSIONS

The obtained catalysts have different characteristic textures. However, a larger specific surface area does not imply better photocatalytic activity. The results indicate that the calcination temperature has an influence on the discoloration of reactive blue 5G dye. The oxides CeO<sub>2</sub> and Al<sub>2</sub>O<sub>3</sub> showed low catalytic activity. However, the CeO<sub>2</sub>-TiO<sub>2</sub>-Al<sub>2</sub>O<sub>3</sub> mixed oxide gave results similar to TiO<sub>2</sub>, with 96% and 100% discoloration, respectively, for all the calcination temperatures. The addition of Fe and Ag to the mixed oxide increased the rate of discoloration of reactive blue 5G dye. The only

exception was the non-calcined sample Ag/CeO<sub>2</sub>-TiO<sub>2</sub>-Al<sub>2</sub>O<sub>3</sub>, which presented 97.7% discoloration.

## REFERENCES

- Chen, D.-W., Ray, A. K., Photocatalytic kinetics of phenol and its derivatives over UV irradiated TiO<sub>2</sub>. *Appl. Catal., B: Environ.*, 23, 143 (1999).
- Colpini, L. M. S., Alves, H. J., Santos, O. A. A., Costa, C. M. M., Discoloration and degradation of textile dye aqueous solutions with titanium oxide catalysts obtained by sol-gel method. *Dyes and Pigments*, 76, 525 (2008).

- Houas, A., Lachheb, H., Ksibi, M., Elaloui, E., Guillard, C., Hermann J. M. Photocatalytic degradation pathway of methylene blue in water. *Appl. Catal., B: Environ.*, 31, 145 (2001).
- JCPDS, Internacional Centre for Diffraction Data. PCPDFWIN, 130 (1997).
- Kansal, S. K., Singh, M., Sud, D., Studies on photodegradation of two commercial dyes in aqueous phase using different photocatalysts. *Journal of Hazardous Materials*, 141, 581 (2007).
- Konstantinou, I. K., Albanis T. A., TiO<sub>2</sub>-assisted photocatalytic degradation of zo dyes in aqueous solution: kinetic and mechanistic investigations. A review. *Appl. Catal. B: Environ.*, Amsterdam, 49, 1 (2004).
- Lenzi, G. G., Lenzi, M. K., Baesso, M. L., Bento, A. C., Jorge, L. M. M., Santos, O. A. A., Cobalt, nickel and ruthenium-silica based materials synthesized by the sol-gel method. *Journal of Non-Crystalline Solids*, 354, 4811 (2008).
- Molinari, R., Pirillo, F., Falco, M., Loddo, V., Palmisano, L., Photocatalytic degradation of dyes by using a membrane reactor. *Chem. Eng. Process*, 43, 1103 (2004).
- Özkan, A., Özkan, M. H., Gürkan, R., Akcay, M., Sökmen, M., Photocatalytic degradation of a textile azo dyes, Sirius Gelb GC on TiO<sub>2</sub> or Ag-TiO<sub>2</sub> particles in the absence and presence of UV/VIS irradiation: The effects of some inorganic anions on the photocatalysis. *J. Photochem. Photobiol.*, 163, 29 (2004).
- Pelegri, R., Peralta-Zamora, P., Andrade, A. R., Reyes, J., Duran, N., Electrochemically assisted photocatalytic degradation of reactive dyes. *Appl. Catal. B Environ.*, 22, 83 (1999).
- Peralta-Zamora, P., Pereira, C. M., Tiburtius, E. R. L., Moraes, S. G., Rosa, M. A., Minussi, R. C., Durán, N., Decolorization of reactive dyes by immobilized laccase. *Appl. Catal. B Environ.*, 42, 131 (2003).
- Ràfols, C., Barceló, D. Determination of mono- and disulphonated azo dyes by liquid chromatography-atmospheric pressure ionization mass spectrometry. *J. Chromatogr. A.*, 777, 177 (1997).
- Rezaee, A., Taghi Ghaneian, M., Hashemian, S. J., Moussavi, G., Khavanin, A., Ghanizadeh, G., Decolorization of Reactive Blue 19 Dye from Textile Wastewater by UV/H<sub>2</sub>O<sub>2</sub>. *Process Journal of Applied Sciences*, 6, 1108 (2008).
- Souza, M. C. P., M. Sc.Thesis (In Portuguese), Universidade Estadual de Maringá (2009).
- Weber, J., Stickney, V. C., Hydrolysis kinetics of Reactive Blue 19-vinyl sulfone. *Water Res.* 27, 63 (1993).
- Yan, L., De-Zhi, S., Lin, C., Yan-Ping, L., Preparation and characterization of Fe<sub>2</sub>O<sub>3</sub>-CeO<sub>2</sub>-TiO<sub>2</sub>-γAl<sub>2</sub>O<sub>3</sub> catalyst for degradation dye wastewater. *Journal of Environmental Sciences*, 18, 189 (2006).
- Zollinger, H., *Color Chemistry: Synthesis*. 2<sup>nd</sup> Revised Ed., VCH, Wertheimer (1991).